AIP Advances

RESEARCH ARTICLE | OCTOBER 14 2024

Spectral and spatial resolution of an extreme ultraviolet broadband imaging spectrometer based on dispersion-matched zone plates

Ievgeniia Babenko ; Yahia Mostafa ; Zoi Bouza; Oscar O. Versolato ; Muharrem Bayraktar

AIP Advances 14, 105021 (2024)
https://doi.org/10.1063/5.0226426

Articles You May Be Interested In

The spectrum of a 1- μ m-wavelength-driven tin microdroplet laser-produced plasma source in the 5.5–265.5 nm wavelength range

AIP Advances (December 2021)

Production of 13.5 nm light with 5% conversion efficiency from 2 μ m laser-driven tin microdroplet plasma

Appl. Phys. Lett. (December 2023)

Efficient extreme ultraviolet emission by multiple laser pulses

Appl. Phys. Lett. (July 2024)

21 October 2024 09:22:06

Spectral and spatial resolution of an extreme ultraviolet broadband imaging spectrometer based on dispersion-matched zone plates

Cite as: AIP Advances 14, 105021 (2024); doi: 10.1063/5.0226426
Submitted: 1 July 2024 • Accepted: 30 September 2024 •
Published Online: 14 October 2024

Ievgeniia Babenko,[1] Yahia Mostafa,[1,2] Zoi Bouza,[1,2] Oscar O. Versolato,[1,2] and Muharrem Bayraktar[3,a)]

AFFILIATIONS

[1] Advanced Research Center for Nanolithography, Science Park 106, 1098 XG Amsterdam, The Netherlands
[2] Department of Physics and Astronomy, and LaserLaB, Vrije Universiteit Amsterdam, De Boelelaan 1081, 1081 HV Amsterdam, The Netherlands
[3] Industrial Focus Group XUV Optics, MESA+ Institute for Nanotechnology, University of Twente, Drienerlolaan 5, 7522 NB Enschede, The Netherlands

[a)] Author to whom correspondence should be addressed: m.bayraktar@utwente.nl

21 October 2024 09:22:06

ABSTRACT

We present a combined 1D imaging and broadband spectroscopy tool for analyzing laser-produced plasma sources of extreme ultraviolet light using a tapered zone plate that is dispersion-matched to a transmission grating. Specifically, we follow up on prior work [Mostafa *et al.* Opt. Lett. **48**, 4316 (2023)] to obtain the actual spectral and spatial resolution of the imaging spectrometer and compare it to the design values. The imaging spectrometer is shown to have a spectral resolution of 1.2 nm at 13.5 nm, close to its design value, by assessing spectra obtained from carbon laser-produced plasma in a 5–180 nm wavelength band. The spatial resolution was obtained by placing slits near the object plane and back-illuminating the slit with a tin laser-produced plasma and found to be 17(5) μm, somewhat larger than the design specifications but still well within design limits for use for diagnosing plasma.

© 2024 Author(s). All article content, except where otherwise noted, is licensed under a Creative Commons Attribution-NonCommercial 4.0 International (CC BY-NC) license (https://creativecommons.org/licenses/by-nc/4.0/). https://doi.org/10.1063/5.0226426

I. INTRODUCTION

The emission spectrum of extreme ultraviolet (EUV) light sources for state-of-the-art lithography machines is of key importance for the lithographic process.[1,2] EUV light is currently obtained from laser-produced plasma (LPP), in turn generated from microdroplets of tin.[3–6] This tin LPP emits light over a wide wavelength region[7] ranging from the soft x-ray to the visible regime and beyond. Its emission peaks in the 13.5 nm ± 1% "in-band" region where multilayer mirrors can be employed.[7] Out-of-band light in the EUV range may contribute to mirror heating and ionization of ambient gases. Longer-wavelength emission, for example, in the ultraviolet, may still be reflected by the optics and reduce imaging contrast[8,9] if the light indeed is captured by the etendue and is transmitted through limiting apertures. A complete understanding of the plasma emission in both spectral and spatial terms is required to assess the impact of any changes in the plasma "recipe," part of ongoing optimizations, on the overall lithography machine performance. Thus, a combined imaging and spectroscopy approach is required over a wide wavelength range.

Recently, Mostafa *et al.*[10] presented a novel imaging spectrometer operating across a broad 5–80 nm range that would enable obtaining such a complete understanding of plasma emission. This novel device employs a transmission grating in series with a set of one-dimensional (1D) zone plates[11,12] that are individually matched (tapered[13]) to a particular wavelength set by the grating dispersion. It is designed for 2D imaging of plasma light sources in the extreme, vacuum, and deep ultraviolet regimes. However, the precise values for the obtainable spectral and spatial resolution were not addressed and instead, only theoretical, idealized values for the resolution values were provided.

In this work, we employ the developed imaging spectrometer and provide experimental evidence for the spectral and spatial resolution. To obtain the spectral resolution, we laser-irradiate a solid

© Author(s) 2024

carbon target to form a plasma with well-known and well-resolved spectral lines. For the spatial resolution, we employ various slits placed near the object plane and subsequently back-illuminate them with a larger plasma that is laser-generated from solid tin.

For the spatial resolution, we consider a 5–180 nm wavelength band. For the spectral resolution, we focus our studies on the 9–25 nm wavelength range, which is the range in which by far the dominant part of the radiative power sits.

II. EXPERIMENTAL SETUP

Figure 1(a) shows a schematic view of the setup, demonstrating the laser impacting a solid target. In the following, we closely adhere to the description of Ref. 10. In brief, a Nd:YAG laser (Continuum Surelite-I) operating at its fundamental 1.064 μm wavelength irradiates carbon or tin targets mounted onto a 2D translation stage in a vacuum chamber held at 10^{-6} mbar. We irradiate the targets at a 10 Hz repetition rate while regularly moving the stage to prevent hole burning. The laser beam has a temporal FWHM of ~6 ns and a round focus with a spatial FWHM of 60 μm achieved using a lens with a focal length $f_l = 300$ mm. We set the laser power density in the range $1–10 \times 10^{11}$ W/cm^2 for the measurements shown in this work unless otherwise specified.

The imaging spectrometer is mounted at −30° with respect to the laser beam propagation axis [cf. Fig. 1(a)]. Figures 1(b) and 1(c) show the spectroscopy and the imaging axis, respectively. At a distance $p_1 = 53$ cm, a slit with a width of $A = 150$ μm is used in combination with a 780 lines/mm transmission diffraction grating to disperse the light. The diffracted light impacts a set of 1D-wavelength-tapered zone plates at a distance $p_2 = 5$ cm from the diffraction grating. The zone plates image the source onto a back-illuminated Greateyes CCD (GE2048 512BI UV1) at a distance $q = 110$ cm. The CCD has square pixels with a 13.5 μm edge length. This combination of distances results in a magnification $M = 1.9$. Further design considerations and fabrication process steps were extensively described previously[10] and will not be further addressed in the following.

The slit in front of the grating is constant at 150 μm for all measurements. We note that in prior publications (Refs. 14–16 and references therein), a smaller slit width of 50 μm was used for the measurements with 10 000 lines/mm grating; for ease of internal comparison, a constant 150 μm slit width was used here instead.[10]

Overall, the CDD images show a finite tilt angle of ~1°–2°. The angle is due to the sum of tolerance of the angular alignment of grating vs slit vs zone plate vs CCD camera, with the dominant contribution stemming from the relative angle between grating and CCD. The rotation is corrected before any subsequent analysis is performed by rotating the full image.

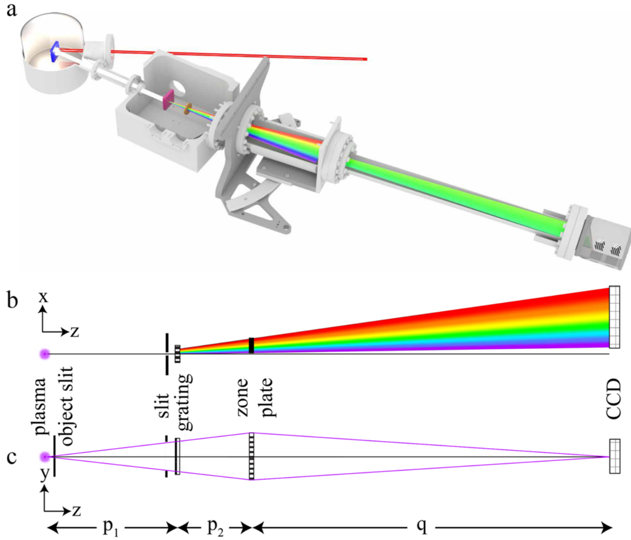

FIG. 1. Experimental setup. (a) Schematic 3D overview of the experimental setup, (b) top–down view showing the spectrometer axis (x-axis), and (c) side view showing the imaging axis (y-axis). Additional slits placed near (3 mm in front of) the object (plasma) plane enable obtaining spatial resolution (shown only in panel (c) for clarity). The figure was modified with permission from Mostafa *et al*., Opt. Lett. **48**, 4316–4319 (2023). © 2023 The Optical Society.

III. RESULTS AND DISCUSSION

A. Spectral resolution

To obtain the spectral resolution of the imaging spectrometer, a carbon target is selected. Plasma produced from a carbon target is well known to exhibit distinct peaks originating from multiply charged carbon ions produced in the plasma. Figure 2(a) presents the results of the measurements taken with 100 mJ laser pulses yielding a laser power density of 5×10^{11} W/cm^2. In these measurements, the Fresnel zone plate was removed from the light path, and no object slit was used (see below Sec. III B). As a side note, adding such a slit near the object plane may improve the spectral resolution, cf. Eq. (1), by reducing ΔS following the equation to obtain the wavelength resolution:

$$\Delta\lambda = \sqrt{\left[\frac{d}{m}\left(\frac{\Delta S + A}{p_1} + \frac{K}{p_2 + q}\right)\right]^2 + \left(\frac{d}{m}\frac{\lambda}{A}\right)^2}. \quad (1)$$

In the current measurements, we use 780 and 3000 lines/mm gratings. Consistent with Fig. 1(c), we use inputs $d = 1.3$ μm and 330 nm as grating periods of 780 and 3000 lines/mm gratings, respectively. Furthermore, we use $m = 1$ as the grating order, $\Delta S = 100$ μm as the estimated source size (see below), and the other parameters p_1, p_2, q, and A as given in Sec. II. Finally, K is the FWHM for the convolution of A across pixel size as explained in Ref. 17. The results from Eq. (1) for the two gratings are plotted as solid curves in Fig. 2(b).

Figure 2(a) shows a typical spectrum for both gratings, exhibiting several well-resolved line features. The most intense line at 13.5 nm (and 11.4–12.1 nm) is only observed at the current high laser intensity [spectra taken at 5× lower energy (not shown in Fig. 2) show no feature at that wavelength] and can be assigned to (highly excited states in) C VI following the NIST database.[18] Other distinct features, such as at 81, 86, 90, and 102 nm wavelength, may tentatively be attributed to C II, and at 95 and 125 nm, we assign lines to neutral C I. These C I and C II lines are also present at the aforementioned 5× lower laser intensity, in line with the assignment to low charge states. The line features mostly comprise multiple electronic transitions, which, however, all lie so close together as to not negatively impact the observed resolution. For the current study,

21 October 2024 09:22:06

© Author(s) 2024

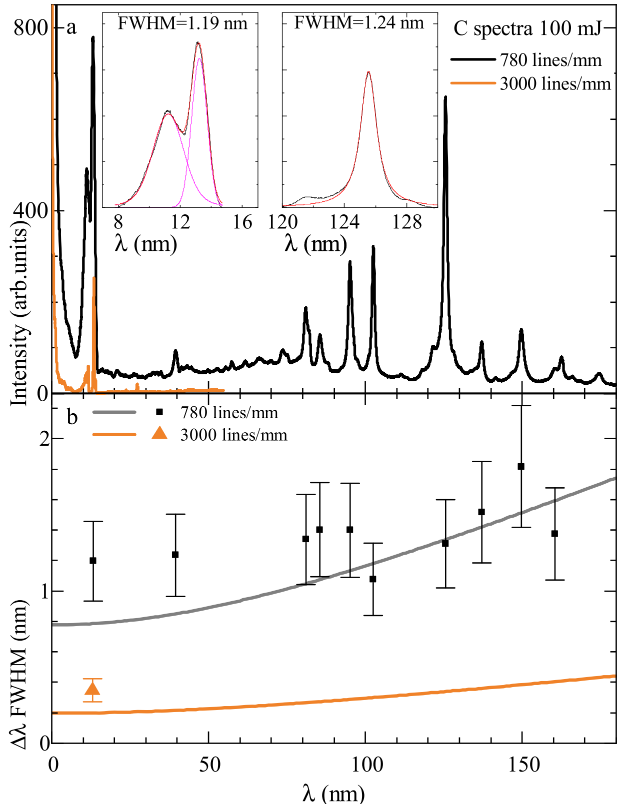

FIG. 2. Spectral resolution. (a) Spectra obtained from C LPP using 100 mJ pulses (see the main text) using 780 and 3000 lines/mm transmission gratings. Insets highlight the quality of the fits for two example cases. (b) Spectral resolution as obtained from fits to spectral features shown in panel (a) for the two gratings (only a single point was obtained for the 3000 lines/mm grating). The solid lines represent predictions from Eq. (1) for the two gratings.

we do not seek a full assignment to all observed transitions, as the objective is to only obtain the width of the distinct line features for calibration purposes. We note that higher diffraction orders are also clearly visible, dominated by the third order (cf. Refs. 7, 10, and 17) for the 780 lines/mm grating and the second order for the 3000 lines/mm grating. The absence of a second-order diffraction in the 780 lines/mm grating is explained by the excellent fabrication quality, which produces a precise 50/50 duty cycle grating that yields no even diffraction orders.[17] Minor aberrations in the fabrication of the 3000 lines/mm grating due to smaller feature sizes are thought to contribute to a less than perfect cancellation of even orders.

Returning to the objective of obtaining line widths, insets (a1) and (a2) show results of fits to line features to highlight the quality of the Voigt fits. We opt for Voigt fits as this enables a more accurate representation for the actual data. The Lorentzian part of the Voigt may originate from the instrumental response function directly or may be due to atomic line broadening in the plasma, with the current resolution not allowing one to single out the cause. We study a more limited wavelength space for the 3000 lines/mm grating, which is set by the acceptance angle of the bellows system (same for the 780 lines/mm grating). Figure 2(b) shows the overview of the fit results at selected, strong, and sufficiently well-separated emission peaks, which for the 3000 lines/mm grating yields but a single entry. We note that the FWHM of the less intense peak below 12 nm (see inset in Fig. 2) is clearly larger than 1.19 nm, due to the existence of the two families of C VI emission lines around 11.38 and 12.05 nm; hence, it is not included in Fig. 2(b). The error bars are of a systematic nature given the dependence of the fit results on the value of the baseline and the precise line shape (Gauss vs Lorentz vs Voigt) that is used for fitting. More specifically, the shown error bars present the averaged relative root-mean-square variation in fit results using (i) Gaussian fit without baseline subtraction, (ii) Gaussian fit with baseline subtraction, or (iii) Voigt fit with baseline subtraction. The statistical uncertainty is negligible in comparison in all cases. Overall, a good agreement between predictions from Eq. (1) and the data are obtained, validating the expected wavelength resolution. Some deviation may be identified for the shortest-wavelength data points for the 780 lines/mm grating with the spectral resolution slightly underperforming with respect to the expectations. We note that the input for ΔS was taken to be 100 μm (in line with Sec. III B below for Sn plasma) but was not obtained directly experimentally for the carbon measurements. Given that the laser pulse energy was reasonably high and that the carbon lines observed mostly originate from low C charge states (residing in colder plasma at the periphery), we may expect significantly larger source sizes ΔS for the current data. In fact, a 200 μm source size would bring all experimental data into excellent agreement with the predictions from Eq. (1).

B. Spatial resolution

The spatial resolution is set by the zone plate dimensions and the spectral resolution of the grating, as it will be explained in the following. The radius $r_{i,n}$ of the nth zone of the ith zone plate, dispersion-matched to the λ_i^{th} wavelength, is determined by

$$r_{i,n} = \sqrt{n\lambda_i\left(f + \frac{n\lambda_i}{4}\right)} \quad \text{with} \quad \lambda_i = d\frac{x_i}{\sqrt{p_2^2 + x_i^2}}, \tag{2}$$

where f is the focal distance, d is the grating period of the 780 lines/mm grating, and p_2 and q are as previously described. The spatial resolution of the imaged source, ignoring wavelength bandwidth considerations, is determined by

$$\Delta w = \lambda f / 2r_N. \tag{3}$$

To maintain near-diffraction-limited performance, the magnitude of the focus shift Δf due to the finite wavelength resolution $\Delta\lambda$ (theoretically being 0.8 nm at 13.5 nm for the used grating) should be less than the depth of focus (DOF) of the system. This sets a limit on the useful number of zones of the ZP given by $N \leq \lambda/\Delta\lambda$. Any zones beyond this number do not improve the spatial resolution. In the following, the number of zones N at each wavelength λ_i is set to achieve a constant spatial resolution across all wavelengths, $\Delta w \equiv 10$ μm (this value increases modestly to 12 μm if the wavelength bandwidth is also considered). For the current 780 lines/mm grating, the zone plates were fabricated with a minimum width of ~10 μm (~ Δw), which is sufficient not to be limited in the resolution by the feature size. We note that the design choices are highly interwoven, with a higher resolution grating enabling higher spatial resolution in step with wavelength resolution. Given the capabilities to produce zone widths below 2 μm, a spatial resolution better

21 October 2024 09:22:06

© Author(s) 2024

than 3 μm would be achievable in principle using a 10 000 lines/mm grating. However, higher-resolution gratings would reduce the spectral window provided for a single CCD position, and the current design presents a trade-off among sufficient magnification, spectral range, and resolution, taking into account limitations for the current implementation.

In Fig. 3, the results of the spatial resolution measurements are presented, taken from a Sn plasma that is produced with 40 mJ laser pulses. Figure 3(a) shows a CCD image, spanning an approximate 9–25 nm wavelength range, of the produced plasma in the absence of any slit placed near the object plane. The spatial resolution measurements are focused on this specific wavelength band that can be captured in a single CCD position, avoiding experimental challenges in precise alignment and image stitching at various CCD positions. The horizontal band at the center of the CCD images corresponds to the wavelength-resolved 1D image of the plasma focused by the zone plate. Figure 3(b) shows a vertical lineout of panel (a) at 13.5 nm wavelength. The position labels in Fig. 3 are in terms of the object plane, taking into account the pixel size of 13.5 μm and dividing by the magnification factor 1.9. The approximate width of the central peak in Fig. 3(b) is in the order of 100 μm, which is well above the 5.3 μm spatial resolution (at the object plane) design of the imaging spectrometer.

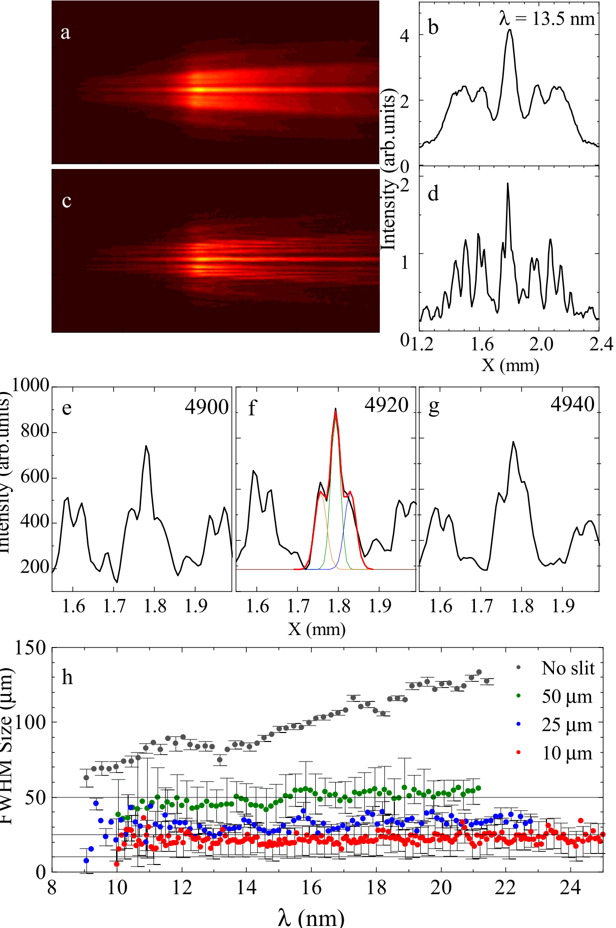

FIG. 3. Spatial resolution. (a) Sample CCD image obtained from Sn LPP (see the main text) with no additional slit installed near the object plane. (b) Vertical lineout of data shown in panel (a) at 13.5 nm wavelength corresponding to the brightest feature. (c) Sample CCD image obtained from Sn LPP with a 25 μm slit installed near the object plane. (d) Vertical lineout of data shown in panel (c) at 13.5 nm wavelength. Panels [(e)–(g)] show vertical lineouts of data shown in panel (b) at 13.5 nm wavelength for various *x*-axis positions of the zone plate to enable finding the optimum focus. Panel (f) also shows a typical fit of three Gaussians and a constant background (see the main text). (h) Spatial resolution as obtained from fits to vertical lineouts from panels (a), without a slit, and (c), with a 50, 25, and 10 μm slit near the object plane. Only every second error bar is plotted for clarity. The solid lines represent the respective slit sizes.

To study spatial resolution, we insert additional slits of various sizes (10, 25, and 50 μm) near the object plane, as close as possible to the plasma. In practice, it was possible to place the additional slit at a 3 mm distance to the plasma to allow irradiating the target without clipping the drive laser beam. Figure 3(c) shows a CCD image with the setup now incorporating a 25 μm slit. Figure 3(d) shows a vertical lineout of panel (c) at 13.5 nm wavelength. The additional features introduced by adding the 25 μm slit comparing Figs. 3(b)–3(d) are explained by the smaller illumination source allowing studying fine features of the zone plate diffraction, in line with the simulations shown in Ref. 10. For optimal imaging of the plasma (or object slit if applicable), a fine adjustment of the distance between the zone plate and plasma (or CCD camera) is typically required. However, our setup does not allow such adjustment along the *z*-axis (cf. Fig. 1). In the case of our tapered zone plate aligned behind a dispersive element, the focusing condition can instead be manipulated by translating the zone plate along the *x*-axis which, due to the inherent chromaticity of the zone plate combined with the dispersion of the prior optic element, will enable partly modifying the focusing condition. Figures 3(e)–3(g) showcase the dependence of the imaging on the position of the zone plate along the *x*-axis in an effective through-focus scan. The zone plate position at 4900 (this number, in *μ*m units, is derived from the position encoder of the piezo-motor) is used for fitting as it best resolves the center peak from side bands, that is, the image of the source, cf. Fig. 3(d) for the case of a 25 μm slit. Panel (h) in Fig. 3 shows the FWHM value of the center Gauss from the three-Gaussian fits for the cases without slit and with 10, 25, and 50 μm slits. The error bars are derived from uncertainties of the fits. No further systematic uncertainties are identified or added to the figure. Without a slit, the size of the emitting area is clearly seen to increase with wavelength, in line with previous observations. For completeness, we repeat the interpretation[10] here that the observation is explained considering emission from a hot surface with the temperature reducing away from the core. The center of the plasma is the smallest and hottest region of the plasma, responsible for the emission of the shortest wavelengths, as these are emitted by the higher charge states. Longer wavelengths are expected to be emitted from areas away from the core where the temperature is also lower.

Next, we find that when restricting the source size, for the 50 and 25 μm slit, there is an excellent agreement between the slit size and average extracted value for the resolution, given the results of 49(5) μm (for the 50 μm slit), which indicates a spatial resolution better than 10(5) μm, and 32(6) μm (for the 25 μm slit) with a 20(8) μm value that is consistent with the value for the larger slit. The smaller 10 μm object slit furthermore yields a consistent value

21 October 2024 09:22:06

© Author(s) 2024

at 20(5) μm value. We thus find a resolution averaging at 17(5) μm, which is somewhat larger than our prior calculations. We attribute this difference to the fact that we are unable to place the object slit at the plasma position (the object plane) but 3 mm away from it toward the grating and CCD. Part of this effective defocusing is negated by carefully aligning the zone plate in x-direction, but it is only possible to fully eliminate it by adjusting the z-distance. Furthermore, the experimentally extracted 1.2 nm spectral resolution was larger than the 0.8 nm theoretical spectral resolution that is used to calculate the theoretical spatial resolution and design the zone plates. Such a larger wavelength resolution causes larger spatial resolution. The extracted spatial resolution is further impacted by the 13.5 μm pixel size being close to the design resolution in the image plane of ~10 μm, which can be improved by having a higher magnification in the future. Separately, finite zone plate fabrication imperfections and remaining (rotation, tilt) misalignments may negatively impact the obtainable spatial resolution. Nevertheless, with the demonstrated imaging resolution combined with spectroscopy, we have produced a valuable, unique tool for diagnosing plasma in broad wavelength ranges.

IV. CONCLUSIONS

We demonstrated the spectral and spatial resolution of a 1D imaging and spectroscopy tool for the analysis of LPP sources of EUV light. The tool combines zone plates with tapered zone widths to match the dispersion of transmission gratings to cover a broad spectral range demonstrated previously in the 5–80 nm range[10] and here in the 9–25 nm range to quantify its spatial resolution. The spatial resolution is found to be 17(5) μm slightly larger than the design specifications, mainly due to alignment challenges in the current implementation but well below the resolution required to diagnose laser-produced plasma (which extends typically several 100 μm[19]). The presented imaging spectrometer has the capability to reach a spatial resolution better than 3 μm, given the zone widths below 2 μm can be fabricated using more advanced microfabrication techniques. Having demonstrated the working principle and quantified the spatial resolution here, the imaging spectrometer may find applications in the plasma light source characterization studies in the nanolithography, metrology, and other short wavelength light source development fields.

ACKNOWLEDGMENTS

We thank John Sheil for helpful discussions on interpreting the carbon spectra and James Byers for his role in setting up and enabling the experiments. This work was conducted at the Advanced Research Center for Nanolithography (ARCNL), a public–private partnership between the University of Amsterdam (UvA), Vrije Universiteit Amsterdam (VU), Rijksuniversiteit Groningen (UG), the Dutch Research Council (NWO), and the semiconductor equipment manufacturer ASML, and was partly financed by "Toeslag voor Topconsortia voor Kennis en Innovatie (TKI)" from the Dutch Ministry of Economic Affairs and Climate Policy. This project has received funding from the European Research Council (ERC) under the European Union's Horizon 2020 research and innovation program under Grant Agreement No. 802648.

AUTHOR DECLARATIONS

Conflict of Interest

The authors have no conflicts to disclose.

Author Contributions

Ievgeniia Babenko: Conceptualization (equal); Data curation (equal); Formal analysis (equal); Investigation (equal); Methodology (equal); Software (equal); Validation (equal); Visualization (equal); Writing – original draft (equal); Writing – review & editing (equal). **Yahia Mostafa**: Conceptualization (equal); Data curation (equal); Formal analysis (equal); Investigation (equal); Methodology (equal); Software (equal); Validation (equal); Visualization (equal); Writing – original draft (equal); Writing – review & editing (equal). **Zoi Bouza**: Conceptualization (equal); Data curation (equal); Formal analysis (equal); Investigation (equal); Methodology (equal); Software (equal); Validation (equal); Visualization (equal); Writing – original draft (equal); Writing – review & editing (equal). **Oscar O. Versolato**: Conceptualization (equal); Data curation (equal); Formal analysis (equal); Funding acquisition (equal); Investigation (equal); Methodology (equal); Project administration (equal); Resources (equal); Software (equal); Supervision (equal); Validation (equal); Visualization (equal); Writing – original draft (equal); Writing – review & editing (equal). **Muharrem Bayraktar**: Conceptualization (equal); Data curation (equal); Formal analysis (equal); Funding acquisition (equal); Investigation (equal); Methodology (equal); Project administration (equal); Resources (equal); Software (equal); Supervision (equal); Validation (equal); Visualization (equal); Writing – original draft (equal); Writing – review & editing (equal).

DATA AVAILABILITY

The data that support the findings of this study are available from the corresponding author upon reasonable request.

REFERENCES

[1] M. M. Waldrop, "The chips are down for Moore's law," Nature **530**, 144–147 (2016).

[2] V. Bakshi, *Photon Sources for Lithography and Metrology* (SPIE Press, 2023).

[3] V. Y. Banine, K. N. Koshelev, and G. H. P. M. Swinkels, "Physical processes in EUV sources for microlithography," J. Phys. D: Appl. Phys. **44**, 253001 (2011).

[4] M. Purvis, I. V. Fomenkov, A. A. Schafgans, M. Vargas, S. Rich, Y. Tao, S. I. Rokitski, M. Mulder, E. Buurman, M. Kats, J. Stewart, A. D. LaForge, C. Rajyaguru, G. Vaschenko, A. I. Ershov, R. J. Rafac, M. Abraham, D. C. Brandt, and D. J. Brown, "Industrialization of a robust EUV source for high-volume manufacturing and power scaling beyond 250 W," in *Extreme Ultraviolet (EUV) Lithography IX*, edited by K. A. Goldberg (International Society for Optics and Photonics, SPIE, 2018), Vol. 10583 pp. 476–485.

[5] H. Mizoguchi, H. Nakarai, T. Abe, K. M. Nowak, Y. Kawasuji, H. Tanaka, Y. Watanabe, T. Hori, T. Kodama, Y. Shiraishi, T. Yanagida, G. Soumagne, T. Yamada, T. Yamazaki, and T. Saitou, *High Power LPP-EUV Source with Long Collector Mirror Lifetime for High Volume Semiconductor Manufacturing*, China Semiconductor Technology International Conference (CSTIC) (IEEE, 2018), pp. 1–7.

[6] O. O. Versolato, "Physics of laser-driven tin plasma sources of EUV radiation for nanolithography," Plasma Sources Sci. Technol. **28**, 083001 (2019).

21 October 2024 09:22:06

© Author(s) 2024

[7] Z. Bouza, J. Byers, J. Scheers, R. Schupp, Y. Mostafa, L. Behnke, Z. Mazzotta, J. Sheil, W. Ubachs, R. Hoekstra, M. Bayraktar, and O. O. Versolato, "The spectrum of a 1-μm-wavelength-driven tin microdroplet laser-produced plasma source in the 5.5–265.5 nm wavelength range," AIP Adv. **11**, 125003 (2021).

[8] K. Liu, Y. Li, F. Zhang, and M. Fan, "Transient thermal and structural deformation and its impact on optical performance of projection optics for extreme ultraviolet lithography," Jpn. J. Appl. Phys. **46**, 6568–6572 (2007).

[9] G. Yang and Y. Li, "Analysis and control of thermal and structural deformation of projection optics for 22-nm EUV lithography," in *Extreme Ultraviolet (EUV) Lithography III* (International Society for Optics and Photonics, 2012), Vol. 8322, p. 83222V.

[10] Y. Mostafa, Z. Bouza, J. Byers, I. Babenko, W. Ubachs, O. O. Versolato, and M. Bayraktar, "Extreme ultraviolet broadband imaging spectrometer using dispersion-matched zone plates," Opt. Lett. **48**, 4316–4319 (2023).

[11] A. V. Baez, "Fresnel zone plate for optical image formation using extreme ultraviolet and soft X radiation," J. Opt. Soc. Am. **51**, 405–412 (1961).

[12] Q. Li, X. Dai, H. Shi, Y. Liu, and L. Zhang, "Phase-type Fresnel zone plate with multi-wavelength imaging embedded in fluoroaluminate glass fabricated via ultraviolet femtosecond laser lithography," Micromachines **12**, 1362 (2021).

[13] L. E. Ocola, J. Maser, S. Vogt, B. Lai, R. Divan, and G. B. Stephenson, "Tapered tilted linear zone plates for focusing hard x-rays," Proc. SPIE **5539**, 165–173 (2004).

[14] L. Behnke, R. Schupp, Z. Bouza, M. Bayraktar, Z. Mazzotta, R. Meijer, J. Sheil, S. Witte, W. Ubachs, R. Hoekstra, and O. O. Versolato, "Extreme ultraviolet light from a tin plasma driven by a 2-μm-wavelength laser," Opt. Express **29**, 4475 (2021).

[15] R. Schupp, L. Behnke, J. Sheil, Z. Bouza, M. Bayraktar, W. Ubachs, R. Hoekstra, and O. O. Versolato, "Characterization of 1- and 2-μm-wavelength laser-produced microdroplet-tin plasma for generating extreme-ultraviolet light," Phys. Rev. Res. **3**, 013294 (2021).

[16] R. Schupp, L. Behnke, Z. Bouza, Z. Mazzotta, Y. Mostafa, A. Lassise, L. Poirier, J. Sheil, M. Bayraktar, W. Ubachs, R. Hoekstra, and O. O. Versolato, "Characterization of angularly resolved EUV emission from 2-μ m-wavelength laser-driven Sn plasmas using preformed liquid disk targets," J. Phys. D: Appl. Phys. **54**, 365103 (2021).

[17] S. J. Goh, H. M. J. Bastiaens, B. Vratzov, Q. Huang, F. Bijkerk, and K. J. Boller, "Fabrication and characterization of free-standing, high-line-density transmission gratings for the vacuum UV to soft X-ray range," Opt. Express **23**, 4421–4434 (2015).

[18] A. Kramida, Y. Ralchenko, J. Reader NIST ASD Team, NIST Atomic Spectra Database (version 5.11), 2023.

[19] Y. Mostafa, L. Behnke, D. Engels, Z. Bouza, J. Sheil, W. Ubachs, and O. Versolato, "Production of 13.5 nm light with 5% conversion efficiency from 2 μm laser-driven tin microdroplet plasma," Appl. Phys. Lett. **123**, 234101 (2023).

21 October 2024 09:22:06

© Author(s) 2024